PCCP



PAPER



Cite this: DOI: 10.1039/d5cp03780h

High thermopower of monolayers and bilayers of C_{60} derivatives

Mohammed Alzanbaqi,† Bashayr Alanazi,† Asma Alajmi,† Colin Lambert ** and Ali Ismael ***

We use density functional theory to study the thermoelectric properties of a gold-molecule-graphene molecular junction formed a fullerene monomer (denoted PTEG-1), comprising a fullerene derivative with a polar triethylene glycol (TEG) pendent group and found that the Seebeck coefficient is +261 μ V K⁻¹. This high positive value for the Seebeck coefficient is marked contrast with the high negative Seebeck coefficient of a gold-dimer-graphene molecular junction containing two anti-aligned PTEG-1 molecules which we found to be -356 μ V K⁻¹. We also computed the Seebeck coefficient of molecule comprising C₆₀ derivative attached to two ethylene glycol chains (denoted PTEG-2) in the presence of *n*-DMBI⁺ doping, which we found to vary between -109 μ V K⁻¹ and -205 μ V K⁻¹, depending on the level of doping. These high values of the Seebeck coefficients with both positive and negative signs suggest that such molecules are ideal candidates for producing scalable gold-molecule-graphene thermoelectric generators.

Received 30th September 2025, Accepted 21st October 2025

DOI: 10.1039/d5cp03780h

rsc.li/pccp

Introduction

Thermoelectric materials can directly convert a temperature difference ΔT into an electrical voltage ΔV^{1-5} and are of great significance for energy conversion technologies. $^{6-10}$ If ΔT is not too large, then the voltage generated is $\Delta V = -S \times \Delta T$, where the constant of proportionality S is the Seebeck coefficient. The pursuit of enhanced thermoelectric efficiency in molecularscale junctionsnanoscale architectures where organic molecules bridge the gap between two metallic electrodes represents a significant endeavour in nanotechnology. 11,12 This field aims to harness quantum effects at the single-molecule level to convert heat directly into electricity. A primary focus of research has been the development of sophisticated strategies to precisely control the electronic structure and transport properties of the molecular core. 13-16 To this end, diverse gating methodologies have been successfully employed. These include electrostatic gating to shift energy levels, chemical modification to tailor molecular orbitals, mechanical manipulation to alter coupling and strain, and electrochemical gating to induce strong field effects and redox processes. Together, these techniques provide a powerful toolkit for optimizing the thermoelectric response and advancing the design of future energy-harvesting devices. 17-23 Additionally, self-assembled molecular layers (SAMs) are particularly effective at forming thermoelectric thin films over large areas.24,25 Such SAMs can be prepared in

junctions with symmetric²⁶ or asymmetric electrodes, which facilitates the assembly of a top electrode.^{27,28} In particular gold is commonly used as a bottom electrode, with graphene as a top electrode, which prevents the formation of short circuits that typically occur with thermally evaporated top electrodes.

Recently, particularly large values of the Seebeck coefficient were reported^{29,30} for molecular layers based on molecules comprising C₆₀ derivative attached to either a single ethylene glycol chain (denoted PTEG-1) or to two ethylene glycol chains (denoted PTEG-2). The asymmetric junctions in which current flowed perpendicular to the plane of the SAM utilised a gold bottom electrode and a liquid metal eutectic Ga-In (EGaIn) top electrode. In particular, measurements were reported of the Seebeck coefficient of a SAM formed from a fullerene monomer (denoted PTEG-1), comprising a fullerene derivative with a polar triethylene glycol (TEG) pendent group, as shown in Fig. 1a. In these assemblies, the C₆₀ buckyball was chemisorbed to the bottom gold electrode, with TEG chains pointing away from the gold surface. These measurements were compared with measurements of the Seebeck coefficient of a selfassembled bilayer (SAB) formed from dimers of the same molecules. In the SAB, the dipole moments of neighbouring molecules were anti-aligned, as shown in Fig. 1b, such that 50% of molecules had their C60 chemisorbed to the bottom gold electrode with TEG chains pointing away from the gold surface and 50% of molecules had their C₆₀ physisorbed to the EGaIn electrode with TEG chains pointing away from the EGaIn surface. Remarkably, the Seebeck coefficient was found to change sign from a large positive value +195 μV K⁻¹ for the monomerbased PTEG-1 SAM to a large negative value $-209 \mu V K^{-1}$ for the

Physics Department, Lancaster University, Lancaster, LA1 4YB, UK. E-mail: c.lambert@lancaster.ac.uk, k.ismael@lancaster.ac.uk
† These authors contributed equally to this work.

Paper PCCP

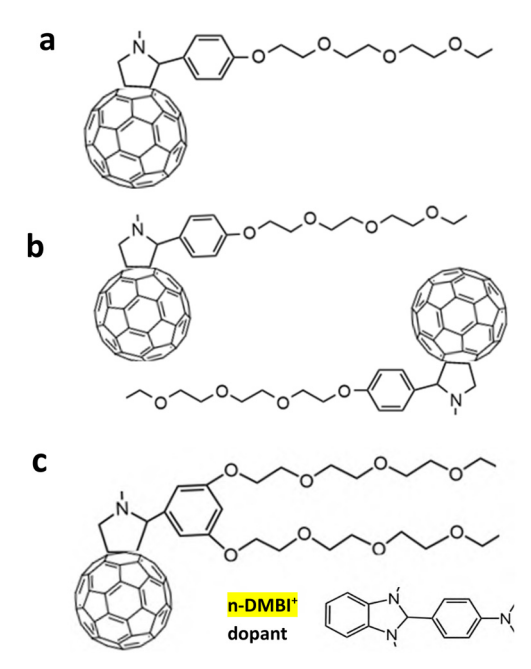


Fig. 1 Chemical structures of the studied C_{60} derivatives: (a) monomer molecule of PTEG-1, consists of fullerene cage with a single triethylene glycol (TEG) chain, (b) a dimer formed from two anti-aligned PTEG-1 molecules. (c) A monomer of PTEG-2 with two triethylene-glycol side chains combined with $n\text{-}\mathsf{DMBI}^+$ dopant.

dimer-based SAB. Additionally, measurements were conducted on the Seebeck coefficient of doped thin films formed from PTEG-1 and PTEG-2. This latter consists of a fullerene derivative with a double triethylene glycol (TEG) pendent group (Fig. 1c below). In these experiments, the thermoelectric properties of PTEG-2 were optimised by doping with counter-ion ((4-(1,3-dimethyl-2,3-dihydro-1H-benzo-imidazol-2-yl)phenyl)dimethylamine n-DMBI) as a dopant (Fig. 1c). The second condition of the second conditi

Since, EGaIn electrodes are not scalable and since they contain an ill-defined oxide layer at the EGaIn-molecule interface, it is of interest to determine if these large Seebeck coefficients and the associated sign change transfer onto more scalable devices, with graphene top electrodes. If the large Seebeck coefficients are an intrinsic property of the junctions, then since the work function of EGaIn is approximately 4.3 eV, which is close to that of graphene at 4.8 eV, one would expect these features to transfer to graphene-based junctions. 32,33 In addition, it is of interest to determine if these large Seebeck coefficients can be translated into molecular-scale junctions, formed from a single molecule or from a molecular dimer. To answer these questions, we examine the thermoelectric properties of the monomer and dimer junctions shown in Fig. 2a, with a gold bottom electrode and a graphene top electrode. As a comparative benchmark, we also compute the Seebeck coefficient of symmetric junctions with gold top electrodes and gold bottom electrodes. In this case (i.e., Au-Au junction), we find that the above sign change does not occur, suggesting that the sign change is not an intrinsic property of molecule, but instead is promoted by the asymmetric nature of the junction electrodes (i.e., Au-Gr junction).

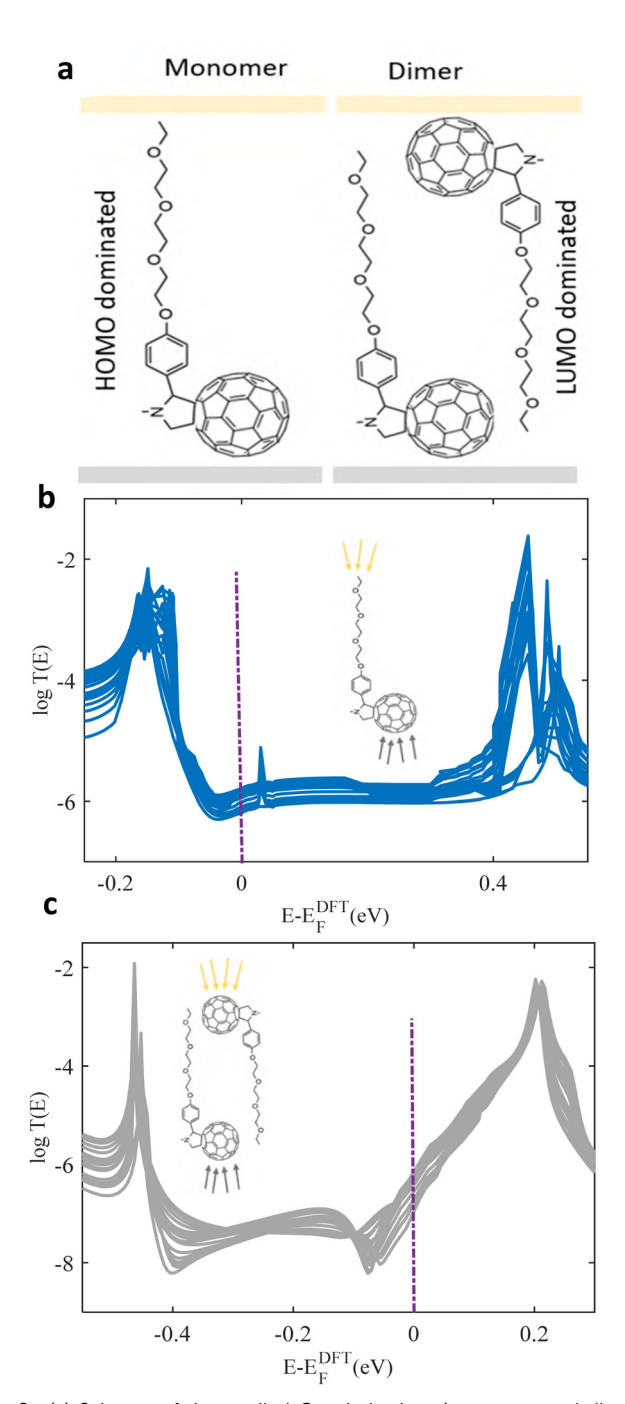


Fig. 2 (a) Scheme of the studied C_{60} derivatives (monomer and dimer) and their junctions. (b) Transmission coefficients T(E) as a function of Fermi energy of molecular junction for Au/monomer PTEG-1/Gr with the average value of 2.4×10^{-6} . (c) Transmission coefficients T(E) as a function of Fermi energy of molecular junction for Au/dimer PTEG-1/Gr with the average value of 4.9×10^{-7} (Note: curves denote different molecular orientations in the junction).

Methods

Our theoretical simulations used the density functional theory (DFT) code SIESTA.³⁴ Geometries of isolated molecules were optimised by relaxing the structures until the forces on the atoms dropped below 0.01 eV Å⁻¹ (for more detail see the SI).

PCCP Paper

A double-zeta plus polarisation orbital basis set, normconserving pseudopotentials and the local density approximation (LDA) for the exchange-correlation function were employed. An energy cutoff of 250 Rydbergs was used to define the real-space grid. Additionally, we computed results using the generalised gradient approximation (GGA), finding that the resulting structures were consistent with those obtained via LDA. 35,36 The thermoelectric properties of these molecules were analysed through a combination of DFT and quantum transport theory. We investigated the monomer PTEG-1, dimer PTEG-1 and PTEG-2 shown in Fig. S1 by first calculating their frontier molecular orbitals and their energy levels, as illustrated in Fig. S2 and S3 for a monomer and dimer of PTEG-1, respectively and Fig. S4 for the PTEG-2. Fig. S5 and S6 show the optimum distance between two fullerene cages C₆₀ (i.e., optimum separation distance X), and between the two chains (i.e., optimum separation distance d, in particular, O atom to O atom), which are essential components of the dimer (for more detail see Section S1.3 in the SI). Since we are employing two different electrode materials (i.e., gold and graphene), it is necessary to compute the optimal binding distance between the two electrodes and terminal ends of the organic molecule. Fig. S7 and S8 display the equilibrium distance corresponding to the energy minimum between the Au electrodes and the molecules vs their Au-molecule distances. Similarly, we calculated the binding energy versus distance between the graphene (Gr) electrode and the molecules, as illustrated in Fig. S9. The minimum energies in these plots correspond to their optimal binding distances and are summarised in Table S1. In Fig. S10, twelve gold-gold junctions are considered in total, Au-monomer-Au, Au-dimer-Au and ten junctions for PTEG-2 with different number of the counter-ion (n-DMBI⁺), specifically 1-5 n-DMBI⁺s at different location and with different orientations (i.e., vertical and horizontal). Fig. S20 and S22 show the corresponding asymmetric junctions (i.e., Gr-Au), for the monomer and dimer of PTEG-1, which also examined in this study.

Results and discussion

The electrical properties of the monomer, dimer of PTEG-1 and PTEG-2 with 1, 2, 3, 4 and 5 counter-ions (n-DMBI⁺) junctions were studied by using density functional theory (DFT) to compute their transmission coefficients, which describe the transport properties of electrons passing through the junction. Fig. S11 and S12 demonstrate their transmission coefficients T(E), while Fig. S13 and S14 present their corresponding Seebeck coefficients S. It should be noted that Au-Au junctions for the PTEG-1 monomer and dimer exhibit opposite signs for S compared to the measured ones, therefore, we repeated the simulations with gold-graphene. The transmission coefficients of the monomer and dimer Au-PTEG-1 derivatives-Gr junctions are displayed in Fig. 2 for a range of different configurations of the PTEG-1 derivatives within the junction (for more detail see Section 1.7 in the SI). Fig. 2b and c, shows that charge transport for monomer PTEG-1 is HOMO dominated, while for dimer

PTEG-1 it is LUMO dominated, as indicted by the dashed-purple lines. Fig. 2b shows transmission coefficients T(E) for different geometry orientations, whose average value at the DFT-predicted Fermi energy is found to be 2.4×10^{-6} for the monomer (Fig. S17). Similarly, Fig. 2c shows transmission coefficients of the dimer, whose average value at the DFT-predicted Fermi energy is 4.09×10^{-7} (Fig. S19).

We find that the energetic positions of the molecular energy levels relative to the electrode Fermi energy^{37,38} are the key features that control the transmission characteristics. The transmission coefficient T(E), depends on the electron energy (E) and the orientation of the molecule. The electronic structure and transmission coefficient of the monomer reveal that the transport is a HOMO-dominated, whereas for the dimer it is LUMO dominated.

The following equation (see *e.g.* Chapter 7 of the textbook³⁹ for a detailed derivation of this equation) shows that the Seebeck coefficient is proportional to the negative slope of $\ln T(E)$ evaluated at the Fermi energy

$$S = -\frac{\pi^2 k_{\rm B}^2 T}{3|e|} \frac{\mathrm{d}}{\mathrm{d}E} \ln(T(E))_{E=E_{\rm Fermi}} \tag{1}$$

where |e| is the magnitude of the electronic charge, and $k_{\rm B}$ is Boltzmann's constant. Therefore, one expects that S is positive when transport is HOMO dominated (*i.e.*, when the HOMO is closest to the Fermi energy) and negative when the LUMO is closest.

This is illustrated by Fig. 3b, which demonstrates a positive Seebeck coefficient for the monomer, with an average value of +261 μ V K⁻¹ (for more information see Fig. S20–S21). Furthermore, it is consistent with Fig. 3c, which shows a negative Seebeck coefficient for the dimer, with average value of –356.8 μ V K⁻¹ (also see Fig. S22 and S23).

These values are summarised in Table 1, along with experimental literature values^{35,40} for the larger systems. Mthembu and Chiechi²⁹ exploited the fullerene moiety of PTEG-1 to bind to Au(111) surface and thus were able to spontaneously form self-assembled monomer (SAMs) of the surface with the TEG chains extending into space. This creates a polar surface to which a second layer of PTEG-1 can be added, resulting in SAM of dimers of anti-aligned PTEG-1s.

In close agreement with the above results, they found that the magnitude and sign of the Seebeck coefficient for the PTEG-1 SAMs is +195 $\mu V~K^{-1}$ while for the self-assembled dimer $-209~\mu V~K^{-1}$ (Table 2).

In what follows, we also calculate the electrical and thermoelectric properties of the PTEG-2 derivative (see 1c), with one, two, three, four and five counter ions (n-DMBI $^+$) as shown in Fig. 4a (for more detail see the SI, Section S1.10 and Fig. S10(4A)–(4E)), to make a comparison with experimental results reported by Liu *et al.*³⁰ We find that the slopes of linear fittings of the T(E) for all the junctions were positive regardless to the number of n-DMBI $^+$ s as illustrated in Fig. 4b (for more detail see Fig. S30–S35); therefore, the Seebeck coefficients of the junctions were negative, as shown in Fig. 4c (Fig. S36–S41). This arises because the Fermi level of the electrode was situated Paper PCCP

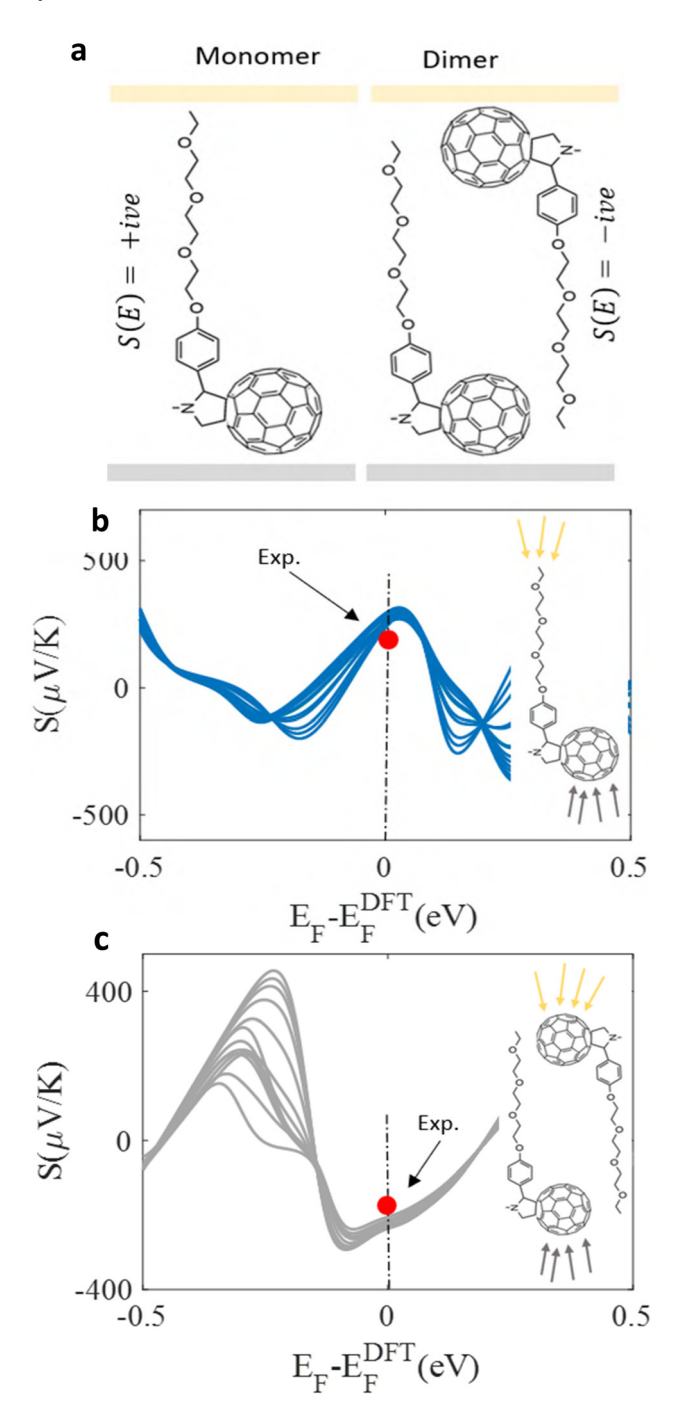


Fig. 3 (a) Schematic of the studied C_{60} derivatives (monomer and dimer) and their junctions. (b) Seebeck coefficients as a function of Fermi energy of molecular junction for Au/PTEG-1 monomer/Gr at different orientations with the average value of +261 μ V K⁻¹. (c) Seebeck coefficients S as a function of Fermi energy of molecular junction at different orientations for Au/PTEG-1 dimer/Gr, with an average value of $-356.8~\mu$ V K⁻¹The red circles indicated the magnitude and the sign of the S in STM measurements. (Note: curves denote different molecular orientations in the junction).

nearest to the LUMO. The Seebeck coefficients of PTEG-2 junctions were -205, -165, -149, -137 and -109 μV K⁻¹ for 1-5 counter ions respectively. Thus, these findings agreed with the experimental trend, which confirms that increasing

Table 1 Thermoelectric properties of the studied PTEG-1 and PTEG-2 derivatives. Measured 35,40 and calculated Seebeck coefficients S in μ V K $^{-1}$ unit, experiment and DFT respectively. PTEG-2 mixed with different n-DMBI $^+$ dopant (**1–5**) counter ions. DFT simulations were chosen at the DFT-predicted Fermi (E_F – $E_F^{\rm DFT}$ = 0 eV)

Junction	$S_{ m (Exp.)}$	$S_{ m (Theo.)}$
Au/PTEG-1 monomer/Gr Au/PTEG-1 dimer/Gr Au/PTEG-2+ 1 n-DMBI ⁺ /Au Au/PTEG-2+ 2 n-DMBI ⁺ /Au Au/PTEG-2+ 3 n-DMBI ⁺ /Au Au/PTEG-2+ 4 n-DMBI ⁺ /Au Au/PTEG-2+ 5 n-DMBI ⁺ /Au	+195 ²⁹ -209 ²⁹ Low concentration (1%) $\sim (-700)^{30}$ ↓ High concentration (10%) $\sim (-200)^{30}$	+262 -357 -205 -165 -149 -137 -109

Table 2 Electrical conductance of the studied PTEG-1 and PTEG-2 derivatives. Measured^{35,40} and calculated G in (G/G_0) unit, experiment and DFT respectively. PTEG-2 mixed with different n-DMBI $^+$ dopant (1-5) counter ions. DFT simulations were chosen at the DFT-predicted Fermi $(E_F - E_F^{\text{DFT}} = 0 \text{ eV})$. For experiment two set of voltage were used +0.5 and -0.5 volt

Junction	$(G/G_0)_{(\text{Exp.})}$	$(G/G_0)_{(Theo.)}$
Au/PTEG-1 monomer/Gr Au/PTEG-1 dimer/Gr	$10^{-8} (\pm 0.5 \text{ volt})^{29}$ $10^{-9} (+0.5 \text{ volt})^{29}$ $10^{-10} (-0.5 \text{ volt})^{29}$	$10^{-5.8} - 10^{-6.3}$ $10^{-7} - 10^{-8}$
$\begin{array}{l} {\rm Au/PTEG\text{-}2+1}\ n\text{-}{\rm DMBI}^{\dagger}/{\rm Au} \\ {\rm Au/PTEG\text{-}2+2}\ n\text{-}{\rm DMBI}^{\dagger}/{\rm Au} \\ {\rm Au/PTEG\text{-}2+3}\ n\text{-}{\rm DMBI}^{\dagger}/{\rm Au} \\ {\rm Au/PTEG\text{-}2+4}\ n\text{-}{\rm DMBI}^{\dagger}/{\rm Au} \\ {\rm Au/PTEG\text{-}2+5}\ n\text{-}{\rm DMBI}^{\dagger}/{\rm Au} \end{array}$	Low concentration (1%) $\sim (10^{-2})^{30}$ \downarrow High concentration (10%) $(10^{-2})^{30}$	$10^{-0.5} 10^{-0.8} 10^{-1.0} 10^{-1.5} 10^{-2.0}$

n-DMBI⁺ concentration causes a decrease in the Seebeck coefficient (see Fig. 4b of ref. 30).

To estimate the expected Seebeck coefficient for a film with random doping concentrations, we shall use the equation below:

$$S = \frac{G_1 S_1 + nG_0 S_0}{G_1 + nG_0} \tag{2}$$

where G_1S_1 are the conductance and Seebeck for high concentration and G_0S_0 for low concentration and $n = \frac{m}{100} - 1$, and m%.

Fig. 5, shows an equivalent comparison between experiment and theory at two different temperatures. These simulations are when the PTEG-2 lays horizontally between the Au–Au junction, this geometry orientation suggests that the dopant n-DMBI $^+$ close to triethylene-glycol side chains prevent the transport via the chains.

We also calculated the transport when the PTEG-2, in vertical positions as shown in Fig. S3A–S3E. In this case, the conductance values are significantly lower $\sim\!10^{-10}$ as demonstrated in Fig. S24–S29, which suggests that for a measurable conductance to appear in in a single-molecule junction, the PTEG-2, should lay in horizontal positions as shown in Fig. 4a above.

Conclusion

The aim of this work has been to determine if the large Seebeck coefficient measured in thicker molecular films contacted to PCCP Paper

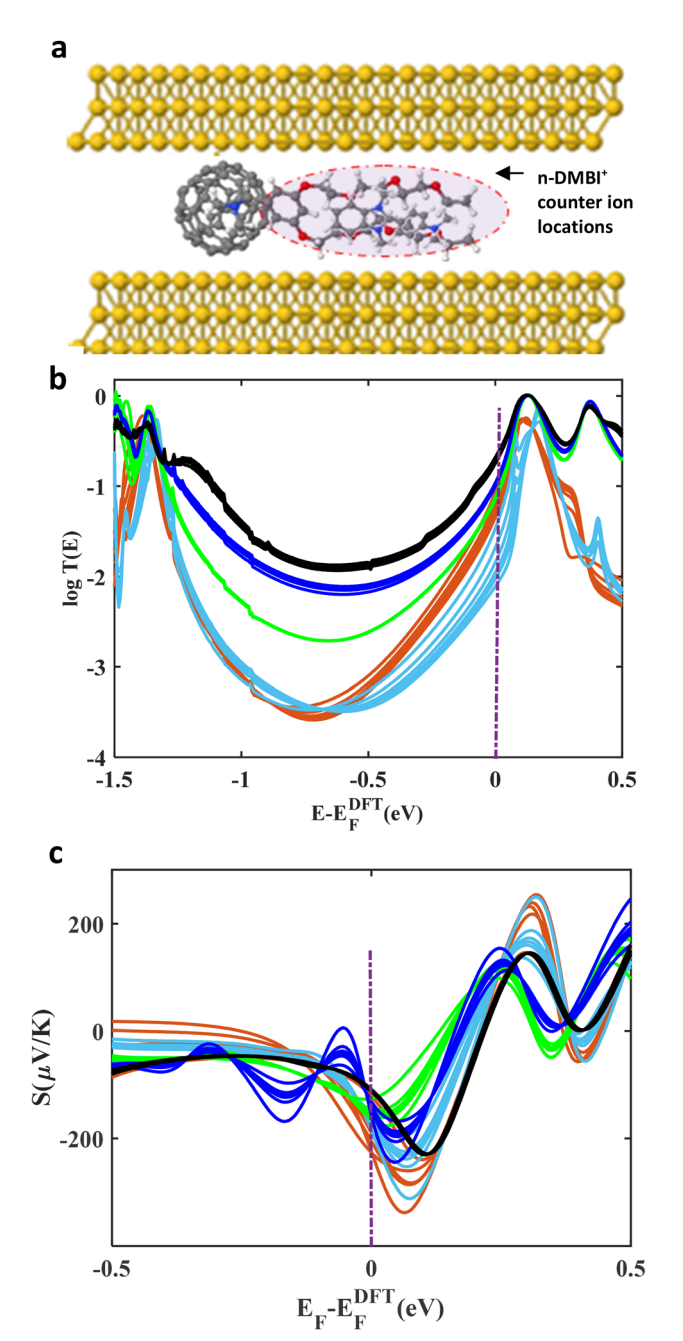


Fig. 4 (a) Scheme illustrates PTEG-2 derivative with different number of $n\text{-}DMBI^+$ counter ions (**1–5**), which acting as the dopant (represented by red-dash elliptical area), in Au–Au junction. (b) Transmission coefficients T(E) as a function of Fermi energy of molecular junction with different numbers of n^-DMBI^+ and as follows: **1** (brown), **2** (light blue), **3** (green), **4** (blue) and **5** (black) respectively. (c) Seebeck coefficients as a function of Fermi energy of molecular junctions for **1**, **2**, **3**, **4** and **5** n^-DMBI^+ counter ions with average values of -205, -165, -149, -137 and 109 μV K^{-1} , respectively.

EGaN can be translated into junctions with graphene top contacts and whether or not these high values could be expected in molecular-scale junctions containing a single molecule or a dimer. We find that the answer to both of these questions is yes. We found that the Seebeck coefficient of PTEG-

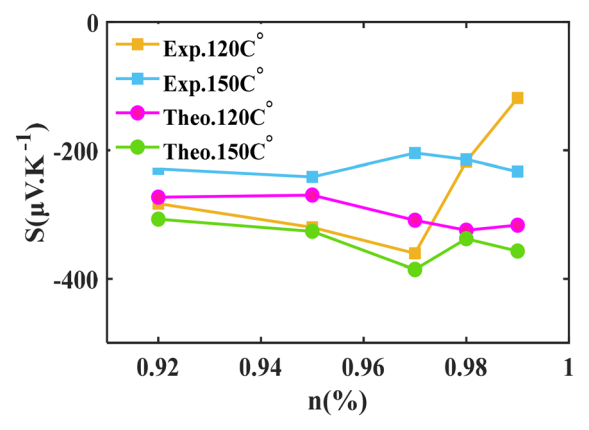


Fig. 5 Seebeck coefficient comparison between experiment and theory at two different temperatures 120 and 150 °C using eqn (2).

1 is +261 μ V K⁻¹, whereas that of a molecular junction containing two anti-aligned PTEG-1 molecules is $-356.8~\mu$ V K⁻¹. We also computed the Seebeck coefficient of molecule comprising C₆₀ derivative attached to two ethylene glycol chains (denoted PTEG-2) in the presence of n-DMBI $^+$ doping, which we found to vary between $-109~\mu$ V K $^{-1}$ and $-205~\mu$ V K $^{-1}$, depending on the level of doping. Our results highlight the impressive sensitivity of thermoelectric performance to doping and molecular alignment. If these features are sufficiently well controlled, our results suggest that PTEG-based molecules are ideal candidates for producing scalable gold-molecule-graphene thermoelectric generators, with large Seebeck coefficients of either sign.

Author contributions

The manuscript was written through contributions of all authors. All authors have given approval to the final version of the manuscript. A. K. I., conceived the research. M. A., A. A. and B. A. carried out the simulations. All co-authors assisted in writing the manuscript. A. K. I., and C. J. L. supervised the research and provided essential contributions to interpreting the results and drafting the manuscript.

Conflicts of interest

There are no conflicts to declare.

Data availability

In this work, we use the following codes. (1) Siesta code used to predict the Hamiltonian of each system used in this study, which is located in https://gitlab.com/siesta-project/siesta/-/releases. (2) GOLLUM software is used to find the website's transmission coefficient. https://www.gollumcode.com/. (3) Conductance, Seebeck, and other parameters are calculated using the own Fortran code available upon request.

Supplementary information (SI) is available. See DOI: https://doi.org/10.1039/d5cp03780h.

Paper PCCP

Acknowledgements

This work was supported by the UK EPSRC (grant QMol EP/ X026876/1). A. K. I. acknowledges the Leverhulme Trust for Early Career Fellowship ECF-2020-638. A. K. I. acknowledge financial support from the Tikrit University (Iraq), and the Iraqi Ministry of Higher Education (SL-20). M. A., A. A. and B. A. are grateful for financial assistance from King Abdulaziz University, Jeddah, Prince Sattam bin Abdulaziz University, Al-Kharj and Northern Border University, Arar (Saudi Arabia), and the Saudi Ministry of Education.

References

- 1 N. Jaziri, A. Boughamoura, J. Müller, B. Mezghani, F. Tounsi and M. Ismail, A comprehensive review of Thermoelectric Generators: Technologies and common applications, *Energy Rep.*, 2020, **6**, 264–287.
- 2 D. Cotfas, A. Enesca and P. Cotfas, Enhancing the performance of the solar thermoelectric generator in unconcentrated and concentrated light, *Renewable Energy*, 2024, **221**, 119831.
- 3 D. Luo, Y. Yan, W.-H. Chen and B. Cao, Exploring the dynamic characteristics of thermoelectric generator under fluctuations of exhaust heat, *Int. J. Heat Mass Transfer*, 2024, 222, 125151.
- 4 W. Yang, C. Jin, W. Zhu, Y. Li, R. Zhang, L. Huang, C. Xie and Y. Shi, Taguchi optimization and thermoelectrical analysis of a pin fin annular thermoelectric generator for automotive waste heat recovery, *Renewable Energy*, 2024, 220, 119628.
- 5 H. Park, Y. Eom, D. Lee, J. Kim, H. Kim, G. Park and W. Kim, High power output based on watch-strap-shaped body heat harvester using bulk thermoelectric materials, *Energy*, 2019, 187, 115935.
- 6 Z. Liang, H. H. Choi, X. Luo, T. Liu, A. Abtahi, U. S. Ramasamy, J. A. Hitron, K. N. Baustert, J. L. Hempel and A. M. Boehm, n-type charge transport in heavily p-doped polymers, *Nat. Mater.*, 2021, 20(4), 518–524.
- 7 A. O. Yusuf, K. N. Baustert, C. D. Pryor and K. R. Graham, The influence of anion size on the thermoelectric properties and Seebeck coefficient inversion in PDPP-4T, MRS Commun., 2024, 14(6), 1127–1133.
- 8 K. Xu, T. P. Ruoko, M. Shokrani, D. Scheunemann, H. Abdalla, H. Sun, C. Y. Yang, Y. Puttisong, N. B. Kolhe and J. S. M. Figueroa, On the origin of Seebeck coefficient inversion in highly doped conducting polymers, *Adv. Funct. Mater.*, 2022, 32(20), 2112276.
- 9 B. Dyaga, A. Lemaire, S. Guchait, H. Zeng, B. Schmaltz and M. Brinkmann, Impact of the dopant location in the semi-crystalline structure of alternated donor–acceptor copolymers on the polarity switching p→ n mechanism, *J. Mater. Chem. C*, 2023, **11**(47), 16554–16562.
- 10 H. Zeng, M. Mohammed, V. Untilova, O. Boyron, N. Berton, P. Limelette, B. Schmaltz and M. Brinkmann, Fabrication of Oriented n-Type Thermoelectric Polymers by Polarity Switching in a DPP-Based Donor-Acceptor Copolymer Doped with FeCl3, Adv. Electron. Mater., 2021, 7(5), 2000880.

11 K. Zou, P. Bai, K. Li, F. Luo, J. Liang, L. Lin, R. Ma, Q. Li, S. Jiang and Q. Wang, Electronic cooling and energy harvesting using ferroelectric polymer composites, *Nat. Commun.*, 2024, 15(1), 6670.

- 12 K. Baheti, J. A. Malen, P. Doak, P. Reddy, S.-Y. Jang, T. D. Tilley, A. Majumdar and R. A. Segalman, Probing the chemistry of molecular heterojunctions using thermoelectricity, *Nano Lett.*, 2008, **8**(2), 715–719.
- 13 S. K. Yee, J. A. Malen, A. Majumdar and R. A. Segalman, Thermoelectricity in fullerene–metal heterojunctions, *Nano Lett.*, 2011, **11**(10), 4089–4094.
- 14 S. K. Lee, T. Ohto, R. Yamada and H. Tada, Thermopower of benzenedithiol and C60 molecular junctions with Ni and Au electrodes, *Nano Lett.*, 2014, 14(9), 5276–5280.
- 15 A. Tan, J. Balachandran, S. Sadat, V. Gavini, B. D. Dunietz, S.-Y. Jang and P. Reddy, Effect of length and contact chemistry on the electronic structure and thermoelectric properties of molecular junctions, *J. Am. Chem. Soc.*, 2011, 133(23), 8838–8841.
- 16 J. Balachandran, P. Reddy, B. D. Dunietz and V. Gavini, Endgroup-induced charge transfer in molecular junctions: effect on electronic-structure and thermopower, *J. Phys. Chem. Lett.*, 2012, 3(15), 1962–1967.
- 17 D. Wu, X.-H. Cao, P.-Z. Jia, Y.-J. Zeng, Y.-X. Feng, L.-M. Tang, W.-X. Zhou and K.-Q. Chen, Excellent thermoelectric performance in weak-coupling molecular junctions with electrode doping and electrochemical gating. Science China Physics, *Mech. Astronomy*, 2020, 63(7), 276811.
- 18 Q. Qi, G. Tian and L. Ma, Enhancing the thermopower of single-molecule junctions by edge substitution effects, *Phys. Chem. Chem. Phys.*, 2024, 26(15), 11340–11346.
- 19 A. Akhtar, U. Rashid, C. Seth, S. Kumar, P. Broekmann and V. Kaliginedi, Modulating the charge transport in metal |molecule| metal junctions via electrochemical gating, *Electrochim. Acta*, 2021, 388, 138540.
- 20 H. Xu, H. Fan, Y. Luan, S. Yan, L. Martin, R. Miao, F. Pauly, E. Meyhofer, P. Reddy and H. Linke, Electrical conductance and thermopower of β-substituted porphyrin molecular junctions—synthesis and transport, *J. Am. Chem. Soc.*, 2023, **145**(43), 23541–23555.
- 21 J. Bai, X. Li, Z. Zhu, Y. Zheng and W. Hong, Single-Molecule Electrochemical Transistors, *Adv. Mater.*, 2021, 33(50), 2005883.
- 22 H. Chen, S. Sangtarash, G. Li, M. Gantenbein, W. Cao, A. Alqorashi, J. Liu, C. Zhang, Y. Zhang and L. Chen, Exploring the thermoelectric properties of oligo (phenylene-ethynylene) derivatives, *Nanoscale*, 2020, 12(28), 15150–15156.
- 23 J. S. Ward and A. Vezzoli, Key advances in electrochemically-addressable single-molecule electronics. Current Opinion in, *Electrochemistry*, 2022, **35**, 101083.
- 24 T. Wang and H. Jeng, Enhancements of thermoelectric performance utilizing self-assembled monolayers in semiconductors, *J. Phys. Chem. Solids*, 2017, **104**, 228–232.
- 25 Z. Chen, S. Qin, J. Jin, Y. Wang, Z. Li, J. Luo, H. Huang, L. Wang and D. Liu, Manipulating carrier concentration by self-assembled monolayers in thermoelectric polymer

PCCP Paper

thin films, ACS Appl. Mater. Interfaces, 2021, 13(27), 32067-32074.

- 26 T. Wink, S. Van Zuilen, A. Bult and W. Van Bennekom, Self-assembled monolayers for biosensors, *Analyst*, 1997, 122(4), 43R-50R
- 27 J. A. Jones, L. A. Qin, H. Meyerson, I. K. Kwon, T. Matsuda and J. M. Anderson, Instability of self-assembled monolayers as a model material system for macrophage/FBGC cellular behavior, *J. Biomed. Mater. Res. Part A*, 2008, **86**(1), 261–268.
- 28 F. Schreiber, Structure and growth of self-assembling monolayers, *Prog. Surf. Sci.*, 2000, **65**(5–8), 151–257.
- 29 C. L. Mthembu and R. C. Chiechi, Self-Assembly Determines Sign of Seebeck Coefficient in Tunneling Junctions Comprising Monolayers and Bilayers of Fullerenes, *Nano Lett.*, 2024, 24(35), 10921–10927.
- 30 J. Liu, B. van der Zee, R. Alessandri, S. Sami, J. Dong, M. I. Nugraha, A. J. Barker, S. Rousseva, L. Qiu and X. Qiu, N-type organic thermoelectrics: demonstration of ZT> 0.3, *Nat. Commun.*, 2020, 11(1), 5694.
- 31 O. Bardagot, C. Aumaître, A. Monmagnon, J. Pécaut, P.-A. Bayle and R. Demadrille, Revisiting doping mechanisms of n-type organic materials with N-DMBI for thermoelectric applications: Photo-activation, thermal activation, and air stability, *Appl. Phys. Lett.*, 2021, **118**(20), 203904.
- 32 X. Wang, A. Ismael, B. Alanazi, A. Al-Jobory, J. Wang and C. J. Lambert, High Seebeck coefficient from isolated oligophenyl arrays on single layered graphene via stepwise assembly, *J. Mater. Chem. C*, 2023, **11**(42), 14652–14660.

- 33 A. Ismael, X. Wang, A. Al-Jobory, S. Ning, T. Alotaibi, B. Alanazi, H. Althobaiti, J. Wang, N. Wei and C. J. Ford, Tuning the electrical conductance of oligo (phenylene-ethynylene) derivatives-PbS quantum-dot bilayers, *J. Mater. Chem. C*, 2024, **12**(35), 14004–14012.
- 34 J. M. Soler, E. Artacho, J. D. Gale, A. García, J. Junquera, P. Ordejón and D. Sánchez-Portal, The SIESTA method for ab initio order-N materials simulation, *J. Phys.: Condens. Matter*, 2002, **14**(11), 2745.
- 35 J. Ye, A. Al-Jobory, Q.-C. Zhang, W. Cao, A. Alshehab, K. Qu, T. Alotaibi, H. Chen, J. Liu and A. K. Ismael, Highly insulating alkane rings with destructive σ-interference, *Sci. China Chem.*, 2022, **65**(9), 1822–1828.
- 36 A. K. Ismael and C. J. Lambert, Molecular-scale thermoelectricity: a worst-case scenario, *Nanoscale Horiz.*, 2020, 5(7), 1073–1080.
- 37 J. E. Greenwald, J. Cameron, N. J. Findlay, T. Fu, S. Gunasekaran, P. J. Skabara and L. Venkataraman, Highly nonlinear transport across single-molecule junctions via destructive quantum interference, *Nat. Nanotechnol.*, 2021, **16**(3), 313–317.
- 38 P. Reddy, S.-Y. Jang, R. A. Segalman and A. Majumdar, Thermoelectricity in molecular junctions, *Science*, 2007, 315(5818), 1568–1571.
- 39 C. J. Lambert, Quantum transport in nanostructures and molecules: an introduction to molecular electronics, IoP Publishing, 2021.
- 40 A. K. Ismael, 20-state molecular switch in a Li@ C60 complex, *ACS Omega*, 2023, **8**(22), 19767–19771.